Moving Target Detection Using Distributed MIMO Radar in Clutter With Nonhomogeneous Power

Pu Wang, *Member, IEEE*, Hongbin Li, *Senior Member, IEEE*, and Braham Himed, *Fellow, IEEE*

***Abstract*—In this paper, we consider moving target detection using a distributed multiple-input multiple-output (MIMO) radar on stationary platforms in nonhomogeneous clutter environments. Our study is motivated by the fact that the multistatic transmit–receive configuration in a distributed MIMO radar causes nonstationary clutter. Specifically, the clutter power for the same test cell may vary significantly from one transmit–receive pair to another, due to azimuth-selective backscattering of the clutter. To account for these issues, a new nonhomogeneous clutter model, where the clutter resides in a low-rank subspace with different subspace coefficients (and hence different clutter power) for different transmit–receive pair, is introduced and the relation to a general clutter model is discussed. Following the proposed clutter model, we develop a generalized-likelihood ratio test (GLRT) for moving target detection in distributed MIMO radar. The GLRT is shown to be a constant false alarm rate (CFAR) detector, and the test statistic is a central and noncentral Beta variable under the null and alternative hypotheses, respectively. Simulations are provided to demonstrate the performance of the proposed GLRT in comparison with several existing techniques.**

***Index Terms*—Generalized likelihood ratio test, moving target detection, multiple-input multiple-output (MIMO) radar, multistatic configuration, nonhomogeneous clutter.**

I. Introduction

MULTIPLE-INPUT multiple-output (MIMO) radar, equipped with multiple transmit and multiple receive antennas along with multiple probing waveforms, has received significant interest in recent years (see [1]–[21] and references therein). Compared with the conventional phased-array radar using one transmit aperture with a single probing waveform, MIMO radars offer a number of unique benefits including higher spatial resolution [4], more degrees of freedom (DOFs) [3], enhanced parameter identifiability [5], better spatial coverage [8], detection diversity gain [10], and possibility of direct application of adaptive array techniques [7]. In general, there are two broad types of array configurations being considered for MIMO radar: one with co-located antennas, [3]–[9], and the other with widely separated antennas [10]–[19]. In this paper, we focus on the latter category, and such radar systems are referred to as distributed MIMO radars. A distributed MIMO radar employs widely separated antennas within the transmit and, respectively, receive aperture, and the transmit antennas probe a radar scene using multiple orthogonal waveforms which are separated at each receive antenna by matched filter processing [10], [12].

A distributed MIMO radar allows one to exploit the *spatial or geometric diversity* to enhance target detection. In particular, radar targets often exhibit significant azimuth-selective backscattering with tens of dB of fluctuation in their radar cross section (RCS) [22]. As such, it would be difficult for a traditional mono-static or bistatic radar with a single transmit–receive site to detect such a target, if the sensors are unfavorably located. The spatial diversity of distributed MIMO radar was first discussed in [10] for stationary target detection and later extended in [12] for moving target detection. The focus of [10] was to establish the detection diversity gain, and the effect of clutter was ignored. Meanwhile, the effect of clutter was included in [12] and [19] for moving target detection where it was shown that distributed MIMO radar systems can provide significant performance gain over traditional phased array radar systems. However, the clutter was assumed to be spatially *homogeneous*, i.e., the clutter covariance matrix is identical for all transmit–receive pairs and for all resolution cells. For adaptive detection, it was suggested to estimate the clutter covariance matrix using training data from adjacent resolution cells due to the homogeneous assumption.

In this paper, moving target detection with a distributed MIMO radar in spatially *nonhomogeneous* clutter environments is considered. Our study is motivated by the fact that multistatic transmit–receive configuration usually causes nonstationary clutter across resolution cells [23] and the fact that the clutter power for the same resolution cell may vary significantly from one transmit–receive pair to another, due to azimuth-selective backscattering of clutter scatterers [22]. To take these issues into consideration, we assume that the clutter power is different from one transmit–receive pair to another and, in addition, from one resolution cell to another, although the clutter shares a common low rank structure (see Section II for details). Using this nonhomogeneous clutter model, we develop a generalized-likelihood ratio test (GLRT). The statistical distributions of the GLRT decision variable under both the null and alternative hypotheses are derived in closed forms. The analytical result shows that the GLRT decision variable under the null hypothesis has a central Beta

Manuscript received November 29, 2010; revised April 15, 2011; accepted June 16, 2011. Date of publication June 27, 2011; date of current version September 14, 2011. The associate editor coordinating the review of this manuscript and approving it for publication was Prof. Visa Koivunen. This work was supported in part by a subcontract with Dynetics, Inc., for research sponsored by the Air Force Research Laboratory (AFRL) under Contract FA8650-08-D-1303.

P. Wang and H. Li are with the Department of Electrical and Computer Engineering, Stevens Institute of Technology, Hoboken, NJ 07030 USA (e-mail: pwang4@stevens.edu; hli@stevens.edu).

B. Himed is with the AFRL/RYMD, Dayton, OH 45433 USA (e-mail: Braham.Himed@wpafb.af.mil).

Color versions of one or more of the figures in this paper are available online at http://ieeexplore.ieee.org.

Digital Object Identifier 10.1109/TSP.2011.2160861

distribution independent of the clutter and noise parameters, which implies that the proposed GLRT is a constant false alarm rate (CFAR) detector. Extensive numerical results are provided to verify our analysis and to compare with other detectors in nonhomogeneous environments.

The remainder of the paper is organized as follows. Our signal model is introduced in Section II. The proposed GLRT detector along with the underlying maximum likelihood estimator are developed in Section III. Section IV contains our statistical analysis of the GLRT detector. Simulation results are provided in Section V. Finally, conclusions are drawn in Section VI.

II. Signal Model

Consider a distributed MIMO radar system with M transmit antennas and N receive antennas. The transmit and receive antennas are on stationary platforms. We use the standard assumption for MIMO radars that the M transmit antennas probe a common area of interest using M orthogonal waveforms [1]–[21]. Pulsed transmission is employed as in standard Doppler radars [22]. Each transmitter sends a succession of K periodic pulses, i.e., K repetitions of an orthogonal waveform, over a coherent processing interval (CPI). Each receiver employs a bank of M matched filters corresponding to the M orthogonal waveforms. The matched filter output is sampled at the pulse rate via *slow-time sampling*. Let $\mathbf{x}_{m,n} \in \mathbb{C}^{K\times 1}$ denote the vector formed by the $K \times 1$ samples of the matched filter output (within a CPI) at the nth receiver matched to the mth transmitter. The problem of interest is to detect the presence/absence of a moving target in the test cell using observations $\{\mathbf{x}_{m,n}\}$.

Specifically, the problem involves the following hypothesis testing:

$$\begin{aligned} H_0 &: \mathbf{x}_{m,n} = \mathbf{c}_{m,n} + \mathbf{w}_{m,n}, \\ H_1 &: \mathbf{x}_{m,n} = \alpha_{m,n}\mathbf{a}(f_{m,n}) + \mathbf{c}_{m,n} + \mathbf{w}_{m,n}, \\ &\qquad n = 1,\ldots,N; m = 1,\ldots,M \end{aligned} \tag{1}$$

where $\mathbf{c}_{m,n}$ denotes the clutter, $\mathbf{w}_{m,n}$ denotes the noise, $\mathbf{a}(f_{m,n})$ is the signal steering vector due to a Doppler frequency $f_{m,n}$, and $\alpha_{m,n}$ is the amplitude of the signal, which is determined by the radar cross section (RCS) of the target. A similar hypothesis testing problem for moving target detection was examined in [12] and [19] and interested readers are referred to their work for additional discussions of the problem setup. The main difference is that homogeneous clutter was considered there, while nonhomogeneous clutter is the focus in the current work, as explained shortly.

The Doppler frequency is due to the presence of a moving target, which is usually unknown for the multistatic receivers. The moving target has a velocity denoted by its x- and y-component $(v_x, v_y) \triangleq \mathbf{v}$, assuming 2-dimensional (2-D) motion. This motion creates a different Doppler frequency for different transmit–receive antenna pair. Using the geometry depicted in Fig. 1, the normalized Doppler frequency $f_{m,n}$ is given by [1], [12], [23]

$$f_{m,n} = \frac{v_x T}{\lambda}(\cos\theta_{tm} + \cos\theta_{rn}) + \frac{v_y T}{\lambda}(\sin\theta_{tm} + \sin\theta_{rn}) \tag{2}$$

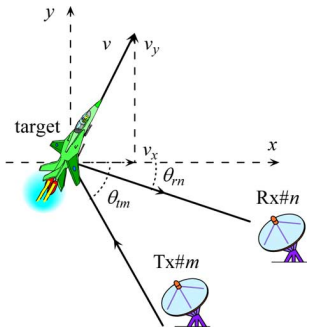

Fig. 1. Transmit–receive pair geometry of a distributed MIMO radar.

where λ denotes the wavelength of the carrier signal and T is the pulse repetition interval (PRI). The signal steering vector, which is formed over the reception of K coherent pulses, is given by

$$\begin{aligned} \mathbf{a}(f_{m,n}) &= [\,1 \quad e^{-j2\pi f_{m,n}} \quad \cdots \quad e^{-j2\pi f_{m,n}(K-1)}\,]^T \\ &\triangleq \mathbf{a}_{m,n}(\mathbf{v}) \end{aligned} \tag{3}$$

where $\mathbf{a}_{m,n}(\mathbf{v})$ is introduced to signify the steering vector for the (m,n)th transmit–receive antenna pair.

The unknown signal amplitude $\alpha_{m,n}$ is related to the RCS of the target. In general, it varies significantly with the aspect angle, due to the azimuth-selective backscattering [10], [12], [22]. As such, in our data model, $\alpha_{m,n}$ is different for different transmit–receive antenna pairs.

The noise $\mathbf{w}_{m,n}$ is assumed to be spatially and temporally white with zero mean and covariance matrix

$$E\left\{\mathbf{w}_{m,n}\mathbf{w}_{n',m'}^H\right\} = \sigma^2\mathbf{I}\delta(n-n')\delta(m-m') \tag{4}$$

where σ^2 denotes the unknown variance of the noise, and $\delta(\cdot)$ is the discrete impulse function.

The clutter components $\mathbf{c}_{m,n}$ contain reflections from stationary (e.g., ground, buildings) and slow moving objects (e.g., grass, forest) within the considered test cell. We assume that the clutter from any transmit–receive pair falls within a subspace which is expanded by the columns of a matrix $\mathbf{H} \in \mathbb{C}^{K\times L}$ (assume $L < K$)

$$\mathbf{H} = [\mathbf{h}(f_1), \mathbf{h}(f_2), \ldots, \mathbf{h}(f_L)] \tag{5}$$

where $\mathbf{h}(f) = [1, e^{-j2\pi f}, \ldots, e^{-j2\pi(K-1)f}]^T$ and $\{f_l\}_{l=1}^L$ are the Doppler frequencies in the low frequency region. As a result, the clutter for a given transmit–receive pair can be expressed as a linear combination of the columns of the matrix $\mathbf{H}$:

$$\mathbf{c}_{m,n} = \mathbf{H}\boldsymbol{\beta}_{m,n} \tag{6}$$

where $\boldsymbol{\beta}_{m,n}$ denotes the $L \times 1$ *unknown* complex coefficient vector associated with the clutter viewed from the aspect of the (m,n)th transmit–receive pair over one CPI and may vary from one CPI to another. The clutter has nonhomogeneous powers for different transmit–receive pairs with distinct clutter coefficients $\boldsymbol{\beta}_{m,n}$, i.e., $\boldsymbol{\beta}_{m,n} \neq \boldsymbol{\beta}_{m',n'}$. Moreover, for a given transmit–receive pair, the clutter coefficients are also different for different

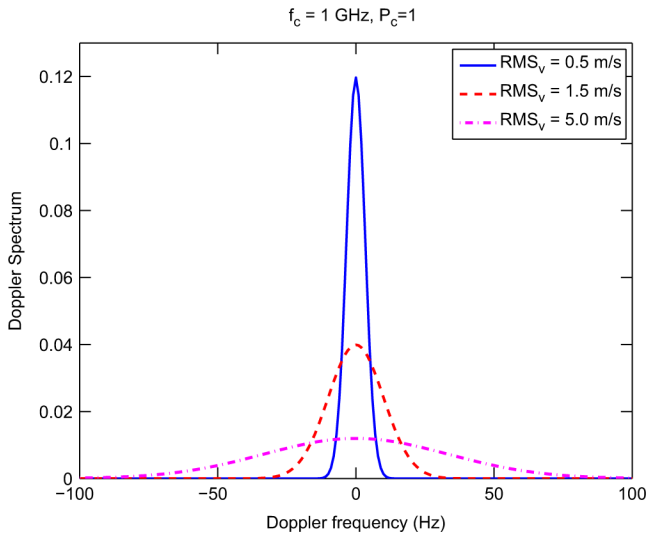

Fig. 2. Clutter power spectral density with $P_c = 1$ and $\lambda = 0.3$ m.

range resolution cells and, therefore, the model is able to represent nonhomogeneous clutter in range. It is noted that the proposed GLRT does not require range training. In Section V, we discuss how to generate nonhomogeneous training signals for other methods, such as the sample covariance matrix-based detector [12], [19], for the distributed MIMO radar.

The proposed subspace clutter model of (6) for the distributed MIMO radar has been motivated by the following considerations. First, as noted previously, the subspace model provides a simple yet flexible tool to approximate the nonhomogeneous clutter from different transmit–receive pairs and from different resolution cells. Second, the subspace clutter model is indeed motivated by the widely accepted fact that the clutter in many practical scenarios has a low-rank structure: $\mathbf{c}_{m,n} \in \mathcal{S}$, where $\mathcal{S}$ denotes a subspace of $\mathbb{C}^{K\times 1}$ with a rank lower than K [24]. Third, the subspace clutter model is also linked to a standard clutter Doppler spectrum model. Specifically, it is generally understood that the clutter is temporally (i.e., across pulses within a CPI) correlated due to internal motions of the clutter scatterers caused by, e.g., wind affecting a forest or grassland. The temporal correlation of the clutter can be characterized by its Doppler power spectral density (PSD) taking the form [19], [22]

$$S_{cc}(f_d) = \frac{P_c\lambda}{2\sqrt{2\pi}\delta_v} e^{-\frac{f_d^2\lambda^2}{8\delta_v^2}} \tag{7}$$

where f_d is the Doppler frequency variable, P_c the clutter power, and δ_v the root mean-square (RMS) of the clutter velocity. Fig. 2 shows the PSD of the clutter as a function of the Doppler frequency in several cases of the RMS of the clutter velocity δ_v when $P_c = 1$ and $\lambda = 0.3$ m. It is seen that the PSD of the clutter is in general located in the low frequency region, and the clutter spread is controlled by δ_v: the smaller the δ_v, the more spiked the clutter PSD. Our subspace based clutter model (6) can be considered as an approximation of (7), by properly selecting the columns, or basis vectors, of $\mathbf{H}$. For example, we can choose $f_l = 0, \pm\frac{\text{PRF}}{K}, \pm 2\frac{\text{PRF}}{K}, \ldots$, where PRF stands for the pulse repetition frequency and $\frac{\text{PRF}}{K}$ denotes the Doppler resolution of using K pulses in a CPI [22]. That is, the columns of the $\mathbf{H}$ form a set of discrete Fourier transform vectors and the number L of such vectors is determined by the Doppler spread of the clutter spectrum. Alternatively, given an upper bound on the bandwidth of the clutter spectrum, we can select f_l uniformly spread across the clutter bandwidth, and L is determined by the rank of the clutter covariance matrix. It should be noted that our clutter model (6) is employed to facilitate algorithmic development. In Section V-C, we will test our detector and other methods by generating clutter from model (7).

III. Generalized-Likelihood Ratio Test

For notational simplicity, define the following vectors and matrices: $\boldsymbol{\alpha} \triangleq [\alpha_{1,1}, \ldots, \alpha_{M,N}]^T \in \mathbb{C}^{MN\times 1}$, $\boldsymbol{\beta} \triangleq [\boldsymbol{\beta}_{1,1}, \ldots, \boldsymbol{\beta}_{M,N}]^T \in \mathbb{C}^{MN\times 1}$, $\mathbf{X} \triangleq [\mathbf{x}_{1,1}, \ldots, \mathbf{x}_{M,N}]^T \in \mathbb{C}^{MN\times K}$. In the following, a GLRT is developed by exploiting the clutter structure. The general form of the test statistic of the GLRT for the problem of interest can be written as

$$\text{GLR} = \frac{\max\limits_{\mathbf{v},\boldsymbol{\alpha},\boldsymbol{\beta},\sigma^2} p_1(\mathbf{X};\mathbf{v},\boldsymbol{\alpha},\boldsymbol{\beta},\sigma^2)}{\max\limits_{\boldsymbol{\beta},\sigma^2} p_0(\mathbf{X};\boldsymbol{\beta},\sigma^2)} \tag{8}$$

where $p_1(\mathbf{X};\mathbf{v},\boldsymbol{\alpha},\boldsymbol{\beta},\sigma^2)$ and $p_0(\mathbf{X};\boldsymbol{\beta},\sigma^2)$ denote the likelihood functions under H_1 and H_0, respectively. Next, we first present the maximum-likelihood (ML) estimates of the unknown parameters under both hypotheses, followed by a summary of the GLRT detector.

A. ML Estimation Under H_1

The ML estimates of the unknown parameters under H_1 are given by (see Appendix I for derivation)

$$\hat{\mathbf{v}} = \arg\max_{\mathbf{v}} \sum_{m,n} \frac{\left|\mathbf{a}_{m,n}^H(\mathbf{v})\mathbf{P}_{\mathbf{H}}^{\perp}\mathbf{x}_{m,n}\right|^2}{\mathbf{a}_{m,n}^H(\mathbf{v})\mathbf{P}_{\mathbf{H}}^{\perp}\mathbf{a}_{m,n}(\mathbf{v})} \tag{9}$$

$$\hat{\alpha}_{m,n} = \frac{\mathbf{a}_{m,n}^H(\hat{\mathbf{v}})\mathbf{P}_{\mathbf{H}}^{\perp}\mathbf{x}_{m,n}}{\mathbf{a}_{m,n}^H(\hat{\mathbf{v}})\mathbf{P}_{\mathbf{H}}^{\perp}\mathbf{a}_{m,n}(\hat{\mathbf{v}})} \tag{10}$$

$$\hat{\boldsymbol{\beta}}_{m,n} = (\mathbf{H}^H\mathbf{H})^{-1}\mathbf{H}^H(\mathbf{x}_{m,n} - \hat{\alpha}_{m,n}\mathbf{a}_{m,n}(\hat{\mathbf{v}})) \tag{11}$$

$$\hat{\sigma}_1^2 = \frac{1}{KMN}\sum_{m,n}\left\|\mathbf{x}_{m,n} - \hat{\alpha}_{m,n}\mathbf{a}_{m,n}(\hat{\mathbf{v}}) - \mathbf{H}\hat{\boldsymbol{\beta}}_{m,n}\right\|^2 \tag{12}$$

where $\mathbf{P}_{\mathbf{H}}^{\perp}$ denotes the projection matrix projecting to the orthogonal complement of the range of $\mathbf{H}$:

$$\mathbf{P}_{\mathbf{H}}^{\perp} = \mathbf{I} - \mathbf{H}(\mathbf{H}^H\mathbf{H})^{-1}\mathbf{H}^H. \tag{13}$$

B. ML Estimation Under H_0

The ML estimates of the unknown parameters under H_0 can be obtained by setting $\boldsymbol{\alpha} = \mathbf{0}$ in (11) and (12), respectively,

$$\hat{\boldsymbol{\beta}}_{m,n} = (\mathbf{H}^H\mathbf{H})^{-1}\mathbf{H}^H\mathbf{x}_{m,n} \tag{14}$$

$$\hat{\sigma}_0^2 = \frac{1}{KMN}\sum_{m,n}\mathbf{x}_{m,n}^H\mathbf{P}_{\mathbf{H}}^{\perp}\mathbf{x}_{m,n}. \tag{15}$$

C. GLR Test Statistic

Using the ML estimates obtained above, it is straightforward to show that the GLR test statistic reduces to

$$\mathrm{GLR} = \left(\frac{\hat{\sigma}_0^2}{\hat{\sigma}_1^2}\right)^{MN} \tag{16}$$

where $\hat{\sigma}_0^2$ is the ML estimate of the noise variance under H_0 in (15), while $\hat{\sigma}_1^2$ is given by (12), which can be simplified as follows:

$$\begin{aligned}\hat{\sigma}_1^2 &= \frac{1}{KMN}\sum_{m,n}\left\|\mathbf{x}_{m,n} - \hat{\alpha}_{m,n}\mathbf{a}_{m,n}(\hat{\mathbf{v}}) - \mathbf{H}\hat{\boldsymbol{\beta}}_{m,n}\right\|^2 \\ &= \hat{\sigma}_0^2 - \frac{1}{KMN}\sum_{m,n}\frac{\left|\mathbf{a}_{m,n}^H(\hat{\mathbf{v}})\mathbf{P}_{\mathbf{H}}^{\perp}\mathbf{x}_{m,n}\right|^2}{\mathbf{a}_{m,n}^H(\hat{\mathbf{v}})\mathbf{P}_{\mathbf{H}}^{\perp}\mathbf{a}_{m,n}(\hat{\mathbf{v}})}.\end{aligned} \tag{17}$$

Dropping the MNth power of (16) and using the monotonicity of the function $f(x) = \frac{1}{(1-x)}$, we have

$$\begin{aligned}T_{\mathrm{GLR}} &= \frac{\max\limits_{\mathbf{v}}\sum\limits_{m,n}\frac{\left|\mathbf{a}_{m,n}^H(\mathbf{v})\mathbf{P}_{\mathbf{H}}^{\perp}\mathbf{x}_{m,n}\right|^2}{\mathbf{a}_{m,n}^H(\mathbf{v})\mathbf{P}_{\mathbf{H}}^{\perp}\mathbf{a}_{m,n}(\mathbf{v})}}{\sum\limits_{m,n}\mathbf{x}_{m,n}^H\mathbf{P}_{\mathbf{H}}^{\perp}\mathbf{x}_{m,n}} \\ &= \frac{\max\limits_{\mathbf{v}}\sum\limits_{m,n}T(\mathbf{v};\mathbf{x}_{m,n})}{KMN\hat{\sigma}_0^2} \underset{H_0}{\overset{H_1}{\gtrless}} \tau\end{aligned} \tag{18}$$

where

$$T(\mathbf{v};\mathbf{x}_{m,n}) = \frac{\left|\mathbf{a}_{m,n}^H(\mathbf{v})\mathbf{P}_{\mathbf{H}}^{\perp}\mathbf{x}_{m,n}\right|^2}{\mathbf{a}_{m,n}^H(\mathbf{v})\mathbf{P}_{\mathbf{H}}^{\perp}\mathbf{a}_{m,n}(\mathbf{v})} \tag{19}$$

and τ is a threshold selected to meet a given probability of false alarm.

It is recognized that $T(\mathbf{v};\mathbf{x}_{m,n})$ corresponds to the decision variable of a matched subspace detector [25] computed using the local measurement $\mathbf{x}_{m,n}$, i.e., matched filter output at the nth receive antenna matched to the mth transmit antenna. Hence, our GLRT can be interpreted as consisting of 1) local matched subspace detection; 2) noncoherent combining using local decision variables of all transmit–receive pairs; 3) selecting the velocity yielding the largest noncoherent sum; and 4) declaring H_1 is true if the largest noncoherent sum is "significant" compared with the white noise variance estimate under H_0. Clearly, how "significant" the noncoherent sum should be depends on the selected test threshold τ or, equivalently, the probability of false alarm. In Section IV, we provide a statistical analysis of the GLRT detector, which can be employed to select τ and compute the corresponding probability of detection for this detector.

D. Sample Covariance Matrix Based Detector

The GLRT is notably different from the sample covariance matrix (SCM) based detector introduced in [12] and [19]:

$$T_{\mathrm{SCM}} = \max_{\mathbf{v}}\sum_{m,n}\frac{\left|\mathbf{a}_{m,n}^H(\mathbf{v})\hat{\mathbf{C}}_{m,n}^{-1}\mathbf{x}_{m,n}\right|^2}{\mathbf{a}_{m,n}^H(\mathbf{v})\hat{\mathbf{C}}_{m,n}^{-1}\mathbf{a}_{m,n}(\mathbf{v})} \underset{H_0}{\overset{H_1}{\gtrless}} \tau_{\mathrm{SCM}} \tag{20}$$

where τ_{SCM} is a threshold for a given probability of false alarm, and $\hat{\mathbf{C}}_{m,n}$ is the sample covariance matrix computed from K_t *homogeneous* training signals $\mathbf{x}_{m,n,k_t} \in \mathbb{C}^{K\times 1}$, $k_t = 1,2,\ldots,K_t$, for the (m,n)th transmit–receive pair:

$$\hat{\mathbf{C}}_{m,n} = \frac{1}{K_t}\sum_{k_t=1}^{K_t}\mathbf{x}_{m,n,k_t}\mathbf{x}_{m,n,k_t}^H. \tag{21}$$

To ensure that the sample covariance matrix is full rank, $K_t > K$ training signals are required for each transmit–receive pair. In general, $K_t = 2K$ training signals are needed for a reasonable performance. As such, the SCM detector (20) requires about $2KMN$ training signals in total, which may be difficult to fulfill in a nonhomogeneous distributed MIMO radar environment. In contrast to the SCM detector, the proposed GLRT requires no training and is well suited to handle clutter with nonhomogeneous power. It is computationally simpler to implement since the projection matrix $\mathbf{P}_{\mathbf{H}}^{\perp}$ needs to be computed only once, while the SCM detector requires to estimate and invert the sample covariance matrix for each transmit–receive pair.

IV. Performance Analysis

In this section, we provide a statistical analysis of the proposed GLRT detector under the condition that the nonlinear velocity parameter $\mathbf{v}$ is known. This is standard in the analysis of radar signal detection such as space-time adaptive processing (STAP) [24]–[27], where nonlinear target parameters, e.g., angle and Doppler frequency are assumed known. In practical implementation, the uncertainty region of the target parameter space is usually divided into small "cells" and each is tested for the presence of target [22], [24]. We follow the same practice. Our analysis provides a benchmark of the best achievable detection performance when the estimation error of $\mathbf{v}$ is negligible. In Section V, we will provide simulation results for both known $\mathbf{v}$ and unknown $\mathbf{v}$ cases, and make comparison.

The following theorem contains our main result.

Theorem 1: Given the signal model in Section II, the statistical distributions of the GLRT test variable (18) under both the null and alternative hypotheses are

$$T_{\mathrm{GLR}} \sim \begin{cases}\beta_{MN,(K-L-1)MN}, & \text{under } H_0 \\ \beta'_{MN,(K-L-1)MN}(\gamma), & \text{under } H_1\end{cases} \tag{22}$$

where $\beta_{MN,(K-L-1)MN}$ denotes a central Beta distribution with parameters MN and $(K-L-1)MN$ [28, pp. 944–945], and $\beta'_{MN,(K-L-1)MN}(\gamma)$ denotes a noncentral Beta distribution with parameters MN and $(K-L-1)MN$ and noncentrality parameter γ [26], [29]–[31]

$$\gamma = \frac{2}{\sigma^2}\sum_m\sum_n|\alpha_{m,n}|^2(\mathbf{a}_{m,n}^H\mathbf{P}_{\mathbf{H}}^{\perp}\mathbf{a}_{m,n}). \tag{23}$$

The proof of Theorem 1 benefits from two lemmas regarding the distributions of the numerator and denominator of the GLRT decision variable under the H_0 and H_1 hypotheses, respectively. The first lemma is concerned with the distributions of the numerator and denominator under H_0.

Lemma 1: Let the denominator and numerator of the GLRT test variable be denoted by

$$T_{\mathrm{GLR-Den}} \triangleq \sum_{m,n}\mathbf{x}_{m,n}^H\mathbf{P}_{\mathbf{H}}^{\perp}\mathbf{x}_{m,n} \tag{24}$$

$$T_{\mathrm{GLR-Num}} \triangleq \sum_{m,n} T(\mathbf{v};\mathbf{x}_{m,n}) = \sum_{m,n} \frac{\left|\mathbf{a}_{m,n}^H \mathbf{P}_{\mathbf{H}}^{\perp} \mathbf{x}_{m,n}\right|^2}{\mathbf{a}_{m,n}^H \mathbf{P}_{\mathbf{H}}^{\perp} \mathbf{a}_{m,n}}. \quad (25)$$

Under the H_0 hypothesis, they are equivalent to

$$T_{\mathrm{GLR-Den}} = \sum_{m,n} \sum_{k=1}^{K-L} |\omega_{m,n,k}|^2 \quad (26)$$

$$T_{\mathrm{GLR-Num}} = \sum_{m,n} |\omega_{m,n,1}|^2 \quad (27)$$

where $\omega_{m,n,k}$ are zero-mean complex Gaussian variables with variance σ^2 which are independent and identically distributed (i.i.d.) for different m, n, and/or k. Furthermore, under H_0,

$$\frac{2}{\sigma^2} T_{\mathrm{GLR-Den}} \sim \chi^2_{2(K-L)MN} \quad (28)$$

$$\frac{2}{\sigma^2} T_{\mathrm{GLR-Num}} \sim \chi^2_{2MN} \quad (29)$$

where χ^2_J denotes a central Chi-square distribution with J degrees of freedom.

Proof: See Appendix II. ∎

The next lemma addresses the distribution of the numerator and denominator of the GLRT test variable under H_1.

Lemma 2: Under the H_1 hypothesis, the denominator and numerator of the test variable can be expressed as

$$T_{\mathrm{GLR-Den}} = \sum_{m,n} \sum_{k=1}^{K-L} |\zeta_{m,n,k}|^2 \quad (30)$$

$$T_{\mathrm{GLR-Num}} = \sum_{m,n} |\zeta_{m,n,1}|^2 \quad (31)$$

where $\zeta_{m,n,k}$ are complex Gaussian variables with mean $\alpha_{m,n}(\mathbf{a}_{m,n}^H \mathbf{P}_{\mathbf{H}}^{\perp} \mathbf{a}_{m,n})^{\frac{1}{2}}$ and variance σ^2 which are independent for different m, n, and/or k. Furthermore, under H_1,

$$\frac{2}{\sigma^2} T_{\mathrm{GLR-Den}} \sim \chi'^2_{2(K-L)MN}(\gamma) \quad (32)$$

$$\frac{2}{\sigma^2} T_{\mathrm{GLR-Num}} \sim \chi'^2_{2MN}(\gamma) \quad (33)$$

$$\frac{2}{\sigma^2}\left(T_{\mathrm{GLR-Den}} - T_{\mathrm{GLR-Num}}\right) \sim \chi^2_{2(K-L-1)MN} \quad (34)$$

where γ is given by (23) and $\chi'^2_J(\gamma)$ denotes a noncentral Chi-square distribution with J degrees of freedom and noncentrality parameter γ.

Proof: see Appendix III. ∎

Proof of Theorem 1 Under H_0

From Lemma 1, the GLRT test variable T_{GLR} under H_0 is a ratio between two central Chi-square random variables:

$$T_{\mathrm{GLR}} = \frac{\frac{2}{\sigma^2}\sum_{m,n} |\omega_{m,n,1}|^2}{\frac{2}{\sigma^2}\sum_{m,n}\sum_{k=1}^{K-L} |\omega_{m,n,k}|^2}. \quad (35)$$

As shown in Appendix II, the numerator is a portion of the denominator under H_0. We can write

$$T_{\mathrm{GLR}} = \frac{T_{a0}}{T_{a0} + \frac{2}{\sigma^2}\sum_{m,n}\sum_{k=2}^{K-L} |\omega_{m,n,k}|^2} \quad (36)$$

where $T_{a0} \triangleq \frac{2}{\sigma^2}\sum_{m,n} |w_{m,n,1}|^2$. Let

$$S_0 \triangleq \frac{\frac{2}{\sigma^2}\sum_{m,n}\sum_{k=2}^{K-L} |\omega_{m,n,k}|^2}{T_{a0}}. \quad (37)$$

Then the random variable S_0 is the ratio of two independent central Chi-square distributions with $2MN(K-L-1)$ and $2MN$ degrees of freedom (see Lemma 1), respectively. Therefore, it is an F-distribution [28, Ch. 26]. As a result, the above GLRT test variable which can be represented as

$$T_{\mathrm{GLR}} = \frac{1}{1+S_0}, \quad (38)$$

has a central Beta distribution with parameters MN and $(K-L-1)MN$ [26], [29] (also see Proposition 5 of Appendix IV). This completes the proof of the distribution of the GLRT test variable under H_0.

Proof of Theorem 1 Under H_1

Similar to the case of H_0 and from Lemma 2, the GLRT test variable (18) under H_1 can be decomposed as

$$T_{\mathrm{GLR}} = \frac{T_{a1}}{T_{a1} + \frac{2}{\sigma^2}\sum_{m,n}\sum_{k=2}^{K-L} |\zeta_{m,n,k}|^2} = \frac{1}{1+S_1} \quad (39)$$

where

$$T_{a1} \triangleq \frac{2}{\sigma^2}\sum_{m,n} |\zeta_{m,n,1}|^2 \quad (40)$$

$$S_1 \triangleq \frac{\frac{2}{\sigma^2}\sum_{m,n}\sum_{k=2}^{K-L} |\zeta_{m,n,k}|^2}{T_{a1}}. \quad (41)$$

Also from Lemma 2, S_1 is the ratio of a central Chi-square random variable with $2MN(K-L-1)$ degrees of freedom to a non-central Chi-square random variable with $2MN$ degrees of freedom and noncentrality parameter γ. It follows from Proposition 6 of Appendix IV that the T_{GLR} is a noncentral Beta distribution as given by (22). This concludes the proof of Theorem 1.

Given the distributions of the GLRT test variable, we can analytically compute the probability of detection and the probability of false alarm, which is employed in Section V. Meanwhile, we see from the above analysis that the distribution of the GLRT test variable under H_0 is independent of the nuisance parameters, i.e., the clutter power $\boldsymbol{\beta}$ and the noise variance σ^2, and hence, the GLRT detector of (18) is a constant false alarm rate (CFAR) detector.

V. Simulation Results

In this section, computer simulation results are presented to verify the above analysis and compare the performance of

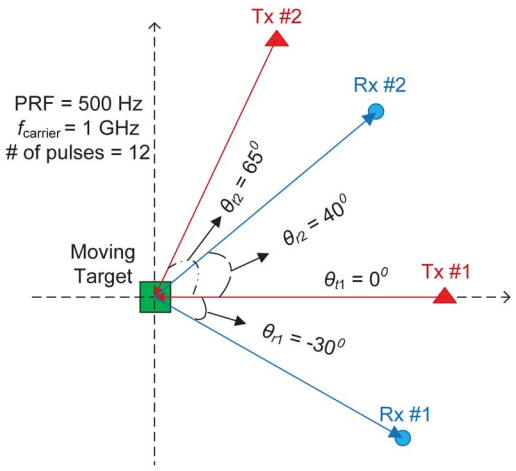

Fig. 3. Distributed MIMO radar configuration used in simulation.

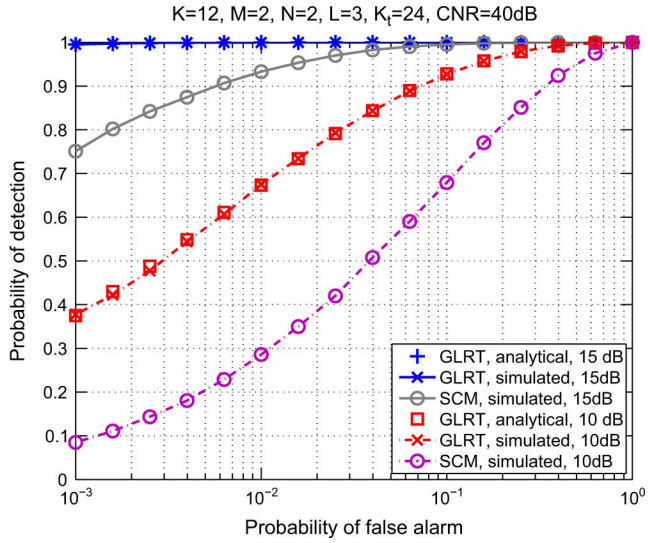

Fig. 4. Receiver-operating-characteristic (ROC) curves for the GLRT and the SCM detectors obtained by computer simulation and analytical computation.

the proposed GLRT with other detectors, including the SCM detector (20) in nonhomogeneous environments. We present detection results when the target velocity $\mathbf{v}$ is known and when $\mathbf{v}$ is unknown and has to be estimated. The signal-to-noise ratio (SNR) and clutter-to-noise ratio (CNR) metrics adopted in this paper are defined as

$$\mathrm{SNR} = \frac{K}{\sigma^2}\sum_{m,n}|\alpha_{m,n}|^2 \tag{42}$$

$$\mathrm{CNR} = \frac{K}{\sigma^2}\sum_{m,n}\boldsymbol{\beta}_{m,n}^H\boldsymbol{\beta}_{m,n}. \tag{43}$$

The distributed MIMO configuration is shown in Fig. 3, which consists of two transmitters at 0° and 65° relative to the target and two receivers at $-30°$ and 40°. It is noted that the configuration is the same as the one in [12] and [19]. The pulse repetition frequency is 500 Hz, the carrier frequency is 1 GHz, the target velocity is 108 km/h, and the number of pulses within a CPI is $K = 12$. The above parameters lead to a normalized target Doppler frequency in (2): $\frac{|\mathbf{v}|T_{\mathrm{PRI}}}{\lambda} = 0.2$.

A. Subspace Clutter With Nonhomogeneous Power

Detection performance in terms of the receiver operating characteristic (ROC) is evaluated for the case of known target velocity to verify our statistical analysis of the GLRT in Section IV. Specifically, the target is assumed to move towards the direction of $\theta = 30°$ in the coordinates of Fig. 3. The amplitude $\boldsymbol{\alpha}$ is one realization of a complex Gaussian random variable with zero mean and unit variance with the squared magnitude equal to $[0.1505, 1.6919, 0.5918, 0.0486]$. The clutters are generated according to (6) with $L = 3$ Doppler frequencies $\{f_l\}_{l=1}^{L=3} = \left[\frac{-1}{K}, 0, \frac{1}{K}\right]$ and with the deterministic clutter coefficients $\boldsymbol{\beta}_{m,n}$. Two cases, $\mathrm{SNR} = 15$ dB and $\mathrm{SNR} = 10$ dB, are considered while fixing $\mathrm{CNR} = 40$ dB.

Fig. 4 shows that the ROC curves for both the GLRT and the SCM obtained by simulation. Also included in Fig. 4 is the ROC curve of the GLRT computed by using the analysis in Section IV. It is seen that the analysis matches well with computer simulation. In addition, the GLRT is observed to attain better detection performance than the SCM detector in the considered nonhomogeneous environment. It is noted that, for each transmit–receive pair, the SCM uses $K_t = 2K = 24$ training signals, $\mathbf{x}_{m,n,k_t}, k_t = 1, \ldots, K_t$, generated as $\mathbf{x}_{m,n,k_t} = \mathbf{H}\boldsymbol{\beta}_{m,n,k_t}$, where $\boldsymbol{\beta}_{m,n,k_t}$ are i.i.d. complex Gaussian vectors with variance determined by the squared magnitude of the entries of $\boldsymbol{\beta}_{m,n}$ of the test signal. Therefore, in each Monte Carlo run, the training signals $\mathbf{x}_{m,n,k_t}$ have nonhomogeneous power with respect to the clutter $\mathbf{c}_{m,n}$ of the test signal. In contrast, the proposed GLRT has no need for training signals.

B. Spatial Diversity

One advantage of MIMO radar over phased-array radar is a so-called spatial diversity that is helpful in target detection from several aspects. First, spatial diversity helps dealing with azimuth-selective backscattering of the target. In particular, while a phased-array radar probes and observes the target from a fixed aspect angle which may be associated with a weak target response, a MIMO radar employs MN geometrically different probe-observe angles, and it is less likely to experience small target amplitude $\alpha_{m,n}$ defined in (1) for all MN transmit–receive pairs [10], [12]. Second, spatial diversity also helps improving moving target detection since for a given target velocity, different transmit–receive pairs see different Doppler frequencies [see (2)] that are less likely to be all small. On the other hand, a phased-array radar sees only one Doppler frequency, which may be small due to an unfavorable radar-target geometry and hard to detect as it resides in the clutter region [1], [12].

In the following, we examine the *spatial diversity* performance of the GLRT and the SCM detector for MIMO radar relative to a representative detector for phased-array radar. To this end, we consider average detection performance averaged over the target moving direction since a fixed direction relative can be particularly favorable or unfavorable to the phased-

array radar (i.e., with maximum or zero Doppler frequency depending on the radar-target geometry). We consider two different cases of target characteristics. In Case A, the moving direction is randomly chosen according to a uniform distribution over the range $[-180^\circ, 180^\circ]$ during each simulation trial, while the target amplitude is constant for all transmit–receive pairs, i.e., *nonfluctuant* target amplitudes. Case B considers not only random target moving direction as in Case A but random (*fluctuant*) target amplitude as well. Specifically, $\alpha_{m,n}$ are generated as complex Gaussian random variables with zero mean and variance $\sigma^2_{\alpha_{m,n}} = 1$. In this case, the SNR is defined as $\text{SNR} = K\sum_{m,n}\sigma^2_{\alpha_{m,n}}/\sigma^2$. The assumption of nonfluctuant target amplitude in Case A allows us to isolate the performance gain due to the distributed transmit–receive configuration from the performance gain from the target fluctuations [19].

For both Cases A and B, the clutter coefficients $\boldsymbol{\beta}_{m,n}$ are randomly generated from trial to trial as a zero-mean complex Gaussian vector with a diagonal covariance matrix $\mathbf{B}_{m,n} = \text{diag}\{B_{m,n,1}, B_{m,n,2}, \ldots, B_{m,n,L}\}$. Similarly to using random target direction/amplitude, the purpose is to provide average detection performance not specific to one set of clutter coefficients. As a result, the clutter $\mathbf{c}_{m,n} = \mathbf{H}\boldsymbol{\beta}_{m,n}$ is a Gaussian distributed vector with zero mean and covariance matrix $\mathbf{H}\mathbf{B}_{m,n}\mathbf{H}^H$. For the SCM detector, the $K_t = 2K$ training signals for the (m,n)th transmit–receive pair are generated as a Gaussian distributed vector with zero mean and covariance matrix $\mathbf{H}\mathbf{B}_{m,n}\mathbf{H}^H$. It should be noted that the clutter of the test signal is random with the same covariance matrix as that of the training signals. As a result, homogeneous training is used for the SCM for these examples.

We consider also using a phased-array (PA) radar in a similar setup for comparison. The phased-array radar has $M = N = 2$ co-located transmit and receive antennas. It employs a standard transmit beamforming on transmit, receive beamforming on receive, and finally Doppler processing by using an adaptive signal detection algorithm. Since the focus here is Doppler processing (for moving target detection), the spatial location (angle) of the target in beamforming is assumed known. Due to transmit–receive beamforming, the receive beamformer output contains a target signal (under H_1) with an effective amplitude $MN\alpha$ and noise with variance $N\sigma^2$, where α denotes the target amplitude and σ^2 the noise variance before receive beamforming [9], [19]. Hence, the SNR for the phased-array radar is M^2 times higher than that of the MIMO radar offered by transmit beamforming [9]. In the following, the clutter for the phased-array radar at the receive beamformer output is generated similar to its counterpart in the MIMO radar, using a covariance matrix $N\mathbf{H}\mathbf{B}\mathbf{H}^H$, where the factor of N is due to receive beamforming. For Doppler processing, we employ the well-known adaptive matched filter (AMF) [27], denoted as the PA-AMF for brevity. The PA-AMF detector uses $K_t = 2K$ homogeneous training signals.

The results of the simulation for Case A are shown in Fig. 5, which indicates the detection performance averaged over randomly moving direction and randomly generated clutter coefficient $\boldsymbol{\beta}_{m,n}$. In this case, with nonfluctuant target amplitude, the proposed GLRT detector outperforms the SCM detectors and the PA-AMF in both cases of known and unknown target

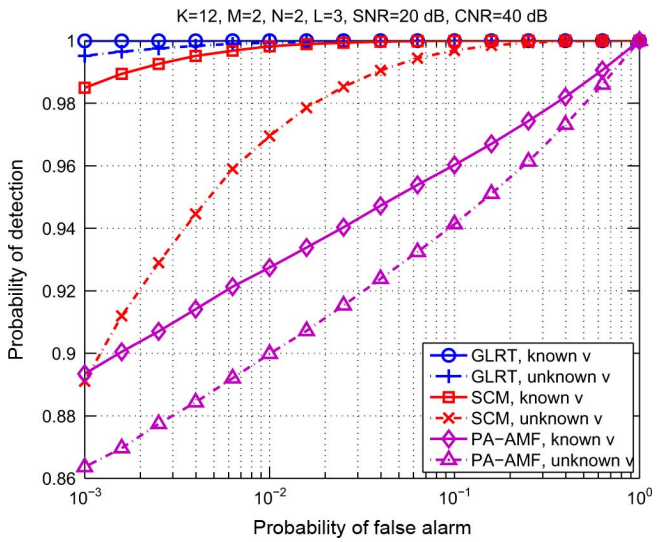

Fig. 5. ROC curves for the GLRT, the SCM, and the PA-AMF detectors with random target moving detection and nonfluctuant target amplitude.

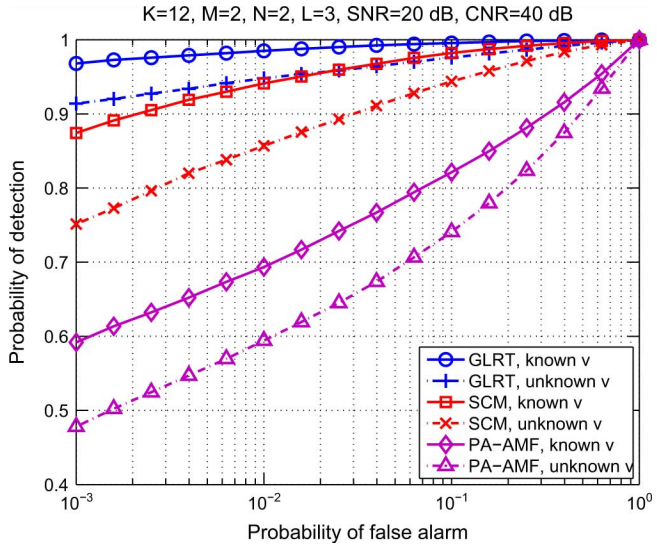

Fig. 6. ROC curves for the GLRT, the SCM, and the PA-AMF detectors with random target moving detection and fluctuant target amplitude.

velocity $\mathbf{v}$. It is also seen that the SCM detector with overall MNK_t training signals provides better detection performance than the PA-AMF, despite the fact the phased-array radar has an SNR gain (due to the aforementioned transmit beamforming) over the MIMO radar. This confirms the significance of spatial diversity provided by the distributed MIMO radar in moving target detection at high SNR, compared with the phased-array radar.

The simulation results for Case B are shown in Fig. 6, which evaluates the average performance against random target moving direction and fluctuant (random) target amplitude. It is seen that the proposed GLRT is still the best one among all considered detectors. Comparing Fig. 5 with Fig. 6, it is noted that the MIMO radar provides even larger spatial diversity than the phased-array radar as larger performance gain observed between the MIMO-based detectors (e.g., the GLRT and SCM detectors) and the phased-array-based PA-AMF detector.

C. General Clutter Model

As shown in Section II, a general clutter model (7) is widely used to model the clutter Doppler characteristics. In this section, we examine the performance of the GLRT in clutter generated according to (7), which in general cannot be exactly represented by the subspace model (6). The purpose is to show the robustness of the proposed GLRT when there is a model mismatch.

According to (7), the temporal correlation function of the clutter can be computed as [19], [22]

$$\Phi(\tau) = \int_{-\infty}^{\infty} \frac{P_c\lambda}{2\sqrt{2\pi}\delta_v} e^{-\frac{f_d^2\lambda^2}{8\delta_v^2}} e^{j2\pi f_d\tau} df_d = P_c e^{-8\pi^2\tau^2\frac{\delta_v^2}{\lambda^2}} \triangleq P_c\phi(\tau). \quad (44)$$

The covariance matrix $\mathbf{C}(P_c)$ is obtained by sampling the above temporal correlation function at $\tau = kT_{\text{PRF}}$, $k = 0, \ldots, K-1$ [19], [22]:

$$\mathbf{C}(P_c) = P_c \begin{pmatrix} \rho(0) & \rho(1) & \cdots & \rho(K-1) \\ \rho(1) & \rho(0) & \cdots & \vdots \\ \vdots & \vdots & \ddots & \rho(1) \\ \rho(K-1) & \cdots & \rho(1) & \rho(0) \end{pmatrix} \quad (45)$$

where P_c is the clutter power and $\rho(k) = \phi(kT_{\text{PRF}})$. To account for the nature of nonhomogeneous clutter power caused by azimuth-selective backscattering, the clutter power P_c associated to the general clutter model is changing over the transmit–receive pairs, i.e., $P_c(m,n) \neq P_c(l,k)$ if $m \neq l, n \neq k$, and also over the training range cells, i.e., $P_c(m,n,\ell) \neq P_c(m,n,\kappa)$ if $\ell \neq \kappa$. As a result, the CNR in this case is computed as $\text{CNR} = K\sum_{m,n}\frac{P_c(m,n)}{\sigma^2}$.

We consider a case with PRF $= 500$ Hz and $\delta_v = 1.5$ m/s for the general clutter model. The other simulation parameters are the same as those used in Fig. 6 of Case B (random moving directions and fluctuant target amplitudes). In order to apply the proposed GLRT, we need a set of Fourier bases, i.e., $\mathbf{H}$ and $\{f_l\}_{l=1}^{L}$, to approximate the clutter spectrum which roughly has a bandwidth $[-25, 25]$ Hz, or equivalently $[-0.05, 0.05]$ in normalized frequency normalized with respect to PRF $= 500$ Hz; see Fig. 2. In this simulation, we choose $\mathbf{H}$ with $L = 3$ normalized frequencies at $\{f_l\}_{l=1}^{3} = [-0.03, 0, 0.03]$ for the proposed GLRT. Meanwhile, for each transmit–receive pair, the SCM detector needs $K_t = 2K$ training signals. Due to nonhomogeneity, the power level $P_c(m,n,\ell)$ may change over the training range cells and thus can be modeled with the compound-Gaussian model [17], where a texture component (the square-root of the power $\sqrt{P_c(m,n,\ell)}$) is used to capture the power variation across range resolution cells. The range training signals is generated with a typical compound-Gaussian model: a K-distributed clutter with a scaling factor 0.5 and a shape factor 2.

The results are shown in Fig. 7 for the proposed GLRT, SCM and the PA-AMF detectors in both cases of known and unknown target velocity. It is seen that, with Fourier bases at $[-0.03, 0, 0.03]$, the GLRT is able to suppress most of the clutter located within the low frequency region and, hence, gives good detection performance. From Fig. 7, it is also observed that the proposed GLRT detector with $L = 3$ outperforms the SCM which may suffer from the power-varying training signals and the PA-AMF which misses spatial diversity and may suffer from a poor fixed aspect angle. Overall, with a proper set of the Fourier bases, the GLRT, without requiring any training signals, can achieve better performance than the SCM detector and the PA-AMF detector. However, compared with Fig. 6, there is a performance loss of the proposed GLRT due to model mismatch.

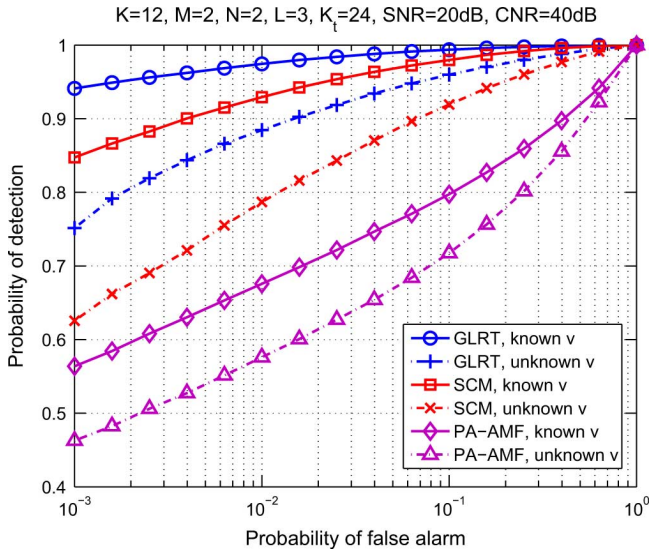

Fig. 7. ROC curves for the GLRT, the SCM and the PA-AMF detectors in clutter generated from the general clutter model (7).

VI. Conclusion

In this paper, we considered the problem of moving target detection using a distributed MIMO radar in nonhomogeneous clutter environments. The clutter was modeled to have a low-rank subspace structure along with a spatially nonhomogeneous clutter power. A new GLRT detector was developed, which performs local matched subspace detection, noncoherent combining using local decision variables of all transmit–receive pairs, target velocity matching, and comparing with a white noise variance estimate. Theoretical analysis was provided to show that the GLRT is a CFAR detector and the distributions of the test variable are central and noncentral Beta distributed under the null and alternative hypotheses, respectively. Simulation results have been provided to verify our analysis. Compared with the SCM detector for distributed MIMO radar and the PA-AMF detector for phased-array radar, our GLRT detector attains better detection performance in clutter environments with nonhomogeneous power. The effect of model mismatch is also investigated.

Appendix I
ML Parameter Estimation

It is noted that the ML estimates under H_0 can be obtained by setting $\boldsymbol{\alpha} = \mathbf{0}$ in the ML estimates under H_1. In the following, we focus herein on the ML estimates under H_1.

According to the signal model described in Section II, the likelihood function under H_1 can be expressed as

$$p_1(\mathbf{X};\mathbf{v},\boldsymbol{\alpha},\boldsymbol{\beta},\sigma^2)=\frac{1}{(\pi\sigma^2)^{KMN}}\exp\Bigg(-\frac{1}{\sigma^2}\sum_{m,n}\big\|\mathbf{x}_{m,n}-\alpha_{m,n}\mathbf{a}_{m,n}(\mathbf{v})-\mathbf{H}\boldsymbol{\beta}_{m,n}\big\|^2\Bigg) \quad (46)$$

where $\|\cdot\|$ denotes the vector 2-norm. Taking the derivative of the log-likelihood $\ln p_1(\mathbf{X};\mathbf{v},\boldsymbol{\alpha},\boldsymbol{\beta},\sigma^2)$ with respect to σ^2 and setting it to zero, we find that the ML estimate of σ^2 is given as

$$\hat{\sigma}_1^2=\frac{1}{KMN}\sum_{m,n}\big\|\mathbf{x}_{m,n}-\alpha_{m,n}\mathbf{a}_{m,n}(\mathbf{v})-\mathbf{H}\boldsymbol{\beta}_{m,n}\big\|^2. \quad (47)$$

Substituting the above estimate back into (46), we find that the ML estimates of the remaining parameters can be determined by minimizing the following cost function

$$\sum_{m,n}\big\|\mathbf{x}_{m,n}-\alpha_{m,n}\mathbf{a}_{m,n}(\mathbf{v})-\mathbf{H}\boldsymbol{\beta}_{m,n}\big\|^2. \quad (48)$$

Let $\mathbf{y}_{m,n}=\mathbf{x}_{m,n}-\alpha_{m,n}\mathbf{a}_{m,n}(\mathbf{v})$. The above cost function is equivalent to

$$\sum_{m,n}\big\|\mathbf{y}_{m,n}-\mathbf{H}\boldsymbol{\beta}_{m,n}\big\|^2. \quad (49)$$

It is easy to show that the ML estimate of $\boldsymbol{\beta}_{m,n}$ is given by

$$\hat{\boldsymbol{\beta}}_{m,n}=(\mathbf{H}^H\mathbf{H})^{-1}\mathbf{H}^H\mathbf{y}_{m,n}. \quad (50)$$

Substitute $\hat{\boldsymbol{\beta}}_{m,n}$ back into the cost function (48), which reduces to

$$\sum_{m,n}\mathbf{y}_{m,n}^T\mathbf{P}_{\mathbf{H}}^{\perp}\mathbf{y}_{m,n}=\sum_{m,n}\left[\mathbf{x}_{m,n}-\alpha_{m,n}\mathbf{a}_{m,n}(\mathbf{v})\right]^H\mathbf{P}_{\mathbf{H}}^{\perp}\times\left[\mathbf{x}_{m,n}-\alpha_{m,n}\mathbf{a}_{m,n}(\mathbf{v})\right] \quad (51)$$

where $\mathbf{P}_{\mathbf{H}}^{\perp}$ is the projection matrix defined in (13). Therefore, the ML estimate of $\alpha_{m,n}$ is given by

$$\hat{\alpha}_{m,n}=\frac{\mathbf{a}_{m,n}^H(\mathbf{v})\mathbf{P}_{\mathbf{H}}^{\perp}\mathbf{x}_{m,n}}{\mathbf{a}_{m,n}^H(\mathbf{v})\mathbf{P}_{\mathbf{H}}^{\perp}\mathbf{a}_{m,n}(\mathbf{v})}. \quad (52)$$

Finally, substituting (52) into (51), we find the ML estimate of $\mathbf{v}$ is given by

$$\hat{\mathbf{v}}=\arg\max_{\mathbf{v}}\sum_{m,n}\frac{\left|\mathbf{a}_{m,n}^H(\mathbf{v})\mathbf{P}_{\mathbf{H}}^{\perp}\mathbf{x}_{m,n}\right|^2}{\mathbf{a}_{m,n}^H(\mathbf{v})\mathbf{P}_{\mathbf{H}}^{\perp}\mathbf{a}_{m,n}(\mathbf{v})}. \quad (53)$$

APPENDIX II
PROOF OF LEMMA 1

Proof of (29): The dependence on velocity $\mathbf{v}$ is henceforth suppressed since it is assumed known. The numerator of the GLRT test variable is defined in (25) and repeated here for easy reference:

$$T_{\mathrm{GLR-Num}}=\sum_{m,n}\frac{\left|\mathbf{a}_{m,n}^H\mathbf{P}_{\mathbf{H}}^{\perp}\mathbf{x}_{m,n}\right|^2}{\mathbf{a}_{m,n}^H\mathbf{P}_{\mathbf{H}}^{\perp}\mathbf{a}_{m,n}}.$$

By recognizing $\mathbf{P}_{\mathbf{H}}^{\perp}\mathbf{x}_{m,n}=\mathbf{P}_{\mathbf{H}}^{\perp}\mathbf{w}_{m,n}$, the (m,n)th term of $T_{\mathrm{GLR-Num}}$ is simplified as

$$\frac{\left|\mathbf{a}_{m,n}^H\mathbf{P}_{\mathbf{H}}^{\perp}\mathbf{w}_{m,n}\right|^2}{\mathbf{a}_{m,n}^H\mathbf{P}_{\mathbf{H}}^{\perp}\mathbf{a}_{m,n}}=\mathbf{w}_{m,n}^H\mathbf{b}_{m,n}\mathbf{b}_{m,n}^H\mathbf{w}_{m,n} \quad (54)$$

where $\mathbf{b}_{m,n}\triangleq\frac{\mathbf{P}_{\mathbf{H}}^{\perp}\mathbf{a}_{m,n}}{(\mathbf{a}_{m,n}^H\mathbf{P}_{\mathbf{H}}^{\perp}\mathbf{a}_{m,n})^{\frac{1}{2}}}$ is a unit-norm vector obtained by projecting $\mathbf{a}_{m,n}$ into $\mathcal{S}_{\mathbf{H}}^{\perp}$ with $\mathcal{S}_{\mathbf{H}}$ denoting the column space of $\mathbf{H}$ and $\mathcal{S}_{\mathbf{H}}^{\perp}$ its orthogonal complement. The eigenvalue decomposition (EVD) of the rank-1 matrix $\mathbf{b}_{m,n}\mathbf{b}_{m,n}^H$ is

$$\mathbf{b}_{m,n}\mathbf{b}_{m,n}^H=\mathbf{Q}\mathrm{diag}\left\{1,0,\ldots,0\right\}\mathbf{Q}^H=\mathbf{q}_1\mathbf{q}_1^H \quad (55)$$

where $\mathbf{Q}\triangleq[\mathbf{q}_1\cdots\mathbf{q}_K]$ contains the K eigenvectors. It follows that $\mathbf{q}_1=\mathbf{b}_{m,n}$ and the remaining $(K-1)$ eigenvectors are arbitrary as long as they are mutually orthogonal and also orthogonal to $\mathbf{b}_{m,n}$. Since $\mathbf{q}_1\in\mathcal{S}_{\mathbf{H}}^{\perp}$, we can choose the $(K-1)$ eigenvectors as

$$\begin{aligned}&\mathbf{q}_k\in\mathcal{S}_{\mathbf{H}}^{\perp},\quad k=2,\ldots,K-L\\&\mathbf{q}_k\in\mathcal{S}_{\mathbf{H}},\quad k=K-L+1,\ldots,K.\end{aligned} \quad (56)$$

By applying the above EVD, (54) is simplified as

$$\begin{aligned}\mathbf{w}_{m,n}^H\mathbf{b}_{m,n}\mathbf{b}_{m,n}^H\mathbf{w}_{m,n}&=\boldsymbol{w}_{m,n}^H\mathrm{diag}\left\{1,0,\ldots,0\right\}\boldsymbol{w}_{m,n}\\&=|w_{m,n,1}|^2\end{aligned} \quad (57)$$

where $\boldsymbol{w}_{m,n}\triangleq\mathbf{Q}^H\mathbf{w}_{m,n}$ and $w_{m,n,1}$ denotes its first element. Since $\mathbf{w}_{m,n}$ has complex Gaussian distribution with zero mean and covariance matrix $\sigma^2\mathbf{I}$, i.e., $\mathbf{w}_{m,n}\sim\mathcal{CN}(\mathbf{0},\sigma^2\mathbf{I})$, we have $\boldsymbol{w}_{m,n}\sim\mathcal{CN}(\mathbf{0},\sigma^2\mathbf{I})$ and hence $w_{m,n,1}\sim\mathcal{CN}(0,\sigma^2)$. Therefore, the (m,n)th term of the GLRT numerator, scaled by $\frac{2}{\sigma^2}$, is a central Chi-square random variable with 2 degrees of freedom:

$$\frac{2}{\sigma^2}|w_{m,n,1}|^2\sim\chi_2^2. \quad (58)$$

It is observed that $w_{m,n,1}$ are i.i.d. for different m and n. Hence, (29) follows.

Proof of (28): The denominator of the GLRT test variable (24) is repeated here for easy reference:

$$T_{\mathrm{GLR-Den}}=\sum_{m,n}\mathbf{x}_{m,n}^H\mathbf{P}_{\mathbf{H}}^{\perp}\mathbf{x}_{m,n}.$$

For the (m,n)th term of $T_{\mathrm{GLR-Den}}$, we have $\mathbf{x}_{m,n}^H\mathbf{P}_{\mathbf{H}}^{\perp}\mathbf{x}_{m,n}=\mathbf{w}_{m,n}^H\mathbf{P}_{\mathbf{H}}^{\perp}\mathbf{w}_{m,n}$. It is known that the projection matrix $\mathbf{P}_{\mathbf{H}}$ has L eigenvalues equal to 0 and $K-L$ eigenvalues identically equal to 1. Therefore, the EVD of $\mathbf{P}_{\mathbf{H}}^{\perp}$ is

$$\mathbf{P}_{\mathbf{H}}^{\perp}=\mathbf{U}\mathrm{diag}\left\{\underbrace{1,\ldots,1}_{K-L},\underbrace{0,\ldots,0}_{L}\right\}\mathbf{U}^H \quad (59)$$

where $\mathbf{u}_k$ is the kth column vector of $\mathbf{U}$ and also the kth eigenvector. From (56), it is convenient to choose

$$\mathbf{u}_1 = \mathbf{q}_1 = \mathbf{b}_{m,n}, \quad \mathbf{u}_k = \mathbf{q}_k, \quad k = 2, \ldots, K-L. \tag{60}$$

As a result, we obtain that

$$\begin{aligned}\mathbf{w}_{m,n}^H \mathbf{P}_{\mathbf{H}}^{\perp} \mathbf{w}_{m,n} &= \boldsymbol{\omega}_{m,n}^H \mathrm{diag}\{1, \ldots, 1, 0, \ldots, 0\} \boldsymbol{\omega}_{m,n} \\ &= \sum_{k=1}^{K-L} |\omega_{m,n,k}|^2 \end{aligned} \tag{61}$$

where $\boldsymbol{\omega}_{m,n} \triangleq \mathbf{U}^H \mathbf{w}_{m,n}$ and $\omega_{m,n,k}$ denotes the kth term of $\boldsymbol{\omega}_{m,n}$. Similarly to (57), we have

$$\frac{2}{\sigma^2} \sum_{k=1}^{K-L} |\omega_{m,n,k}|^2 \sim \chi^2_{2(K-L)}. \tag{62}$$

The distribution (28) follows from the fact that $\omega_{m,n,k}$ are independent for different m and n.

Finally, we examine the relation between the numerator $T_{\mathrm{GLR-Num}}$ and denominator $T_{\mathrm{GLR-Den}}$ of the GLRT test variable. Since $\mathbf{u}_1 = \mathbf{q}_1$ [see (60)], it follows immediately that $w_{m,n,1} = \omega_{m,n,1}$. Hence, $T_{\mathrm{GLR-Num}}$ in (25) is a part of the denominator $T_{\mathrm{GLR-Den}}$ in (24). The proof for Lemma 1 is now complete.

Appendix III
Proof of Lemma 2

Proof of (33): Following the analysis provided under H_0, the derivation under H_1 starts by noting that $\mathbf{P}_{\mathbf{H}}^{\perp}\mathbf{x}_{m,n} = \mathbf{P}_{\mathbf{H}}^{\perp}(\alpha_{m,n}\mathbf{a}_{m,n} + \mathbf{w}_{m,n}) \triangleq \mathbf{P}_{\mathbf{H}}^{\perp}\mathbf{z}_{m,n}$. The (m,n)th term of the GLRT numerator can be rewritten as

$$\begin{aligned}\frac{\left|\mathbf{a}_{m,n}^H \mathbf{P}_{\mathbf{H}}^{\perp} \mathbf{z}_{m,n}\right|^2}{\mathbf{a}_{m,n}^H \mathbf{P}_{\mathbf{H}}^{\perp} \mathbf{a}_{m,n}} &= \boldsymbol{z}_{m,n}^H \mathrm{diag}\{1, 0, \ldots, 0\} \boldsymbol{z}_{m,n} \\ &= |z_{m,n,1}|^2 \end{aligned} \tag{63}$$

where $\boldsymbol{z}_{m,n} = \mathbf{Q}^H \mathbf{z}_{m,n}$, $\mathbf{Q}$ is the same as in (55), and $z_{m,n,1}$ denotes the first element of $\boldsymbol{z}_{m,n}$. Similarly, we have the following intermediate results under the H_1 hypothesis:

$$\begin{aligned}\mathbf{z}_{m,n} &\sim \mathcal{CN}(\alpha_{m,n}\mathbf{a}_{m,n}, \sigma^2\mathbf{I}) \\ \boldsymbol{z}_{m,n} &= \mathbf{Q}^H \mathbf{z}_{m,n} \sim \mathcal{CN}(\alpha_{m,n}\mathbf{Q}^H\mathbf{a}_{m,n}, \sigma^2\mathbf{I}) \\ z_{m,n,1} &\sim \mathcal{CN}(\alpha_{m,n}\mathbf{q}_1^H\mathbf{a}_{m,n}, \sigma^2) \\ &\sim \mathcal{CN}(\alpha_{m,n}(\mathbf{a}_{m,n}^H\mathbf{P}_{\mathbf{H}}^{\perp}\mathbf{a}_{m,n})^{\frac{1}{2}}, \sigma^2) \\ |z_{m,n,1}|^2 &= \Re^2(z_{m,n,1}) + \Im^2(z_{m,n,1}) \\ \Re(z_{m,n,1}) &\sim \mathcal{N}\left(\Re\{\alpha_{m,n}\}(\mathbf{a}_{m,n}^H\mathbf{P}_{\mathbf{H}}^{\perp}\mathbf{a}_{m,n})^{\frac{1}{2}}, \frac{\sigma^2}{2}\right) \\ \Im(z_{m,n,1}) &\sim \mathcal{N}\left(\Im\{\alpha_{m,n}\}(\mathbf{a}_{m,n}^H\mathbf{P}_{\mathbf{H}}^{\perp}\mathbf{a}_{m,n})^{\frac{1}{2}}, \frac{\sigma^2}{2}\right)\end{aligned}$$

where $\Re\{\cdot\}$ and $\Im\{\cdot\}$ denote the real and imaginary parts of the argument, respectively. Therefore, $|z_{m,n,1}|^2$ is a scaled noncentral Chi-square random variable with 2 degrees of freedom and noncentrality parameter $2|\alpha_{m,n}|^2(\mathbf{a}_{m,n}^H\mathbf{P}_{\mathbf{H}}^{\perp}\mathbf{a}_{m,n})/\sigma^2$. Finally, due to the i.i.d. nature of $\mathbf{w}_{m,n}$, the distribution (33) follows.

Proof of (32) and (34): By utilizing the EVD of $\mathbf{P}_{\mathbf{H}}^{\perp}$ [see (59)], the (m,n)th element of $T_{\mathrm{GLR-Den}}$ under H_1 can be expressed as

$$\begin{aligned}\mathbf{x}_{m,n}^H \mathbf{P}_{\mathbf{H}}^{\perp} \mathbf{x}_{m,n} &= \mathbf{z}_{m,n}^H \mathbf{P}_{\mathbf{H}}^{\perp} \mathbf{z}_{m,n} \\ &= \boldsymbol{\zeta}_{m,n}^H \mathrm{diag}\Big\{\underbrace{1, \ldots, 1}_{K-L}, \underbrace{0, \ldots, 0}_{L}\Big\} \boldsymbol{\zeta}_{m,n} \\ &= \sum_{k=1}^{K-L} |\zeta_{m,n,k}|^2 \end{aligned} \tag{64}$$

where $\boldsymbol{\zeta}_{m,n} \triangleq \mathbf{U}^H \mathbf{z}_{m,n}$. From the above equation and the signal model, it is straightforward to show that $2/\sigma^2 \sum_{k=1}^{K-L} |\zeta_{m,n,k}|^2$ has a noncentral Chi-square distribution with $2(K-L)$ degrees of freedom and noncentrality parameter given by

$$\gamma = \frac{2|\alpha_{m,n}|^2 \sum_{k=1}^{K-L} \mathbf{a}_{m,n}^H \mathbf{u}_k \mathbf{u}_k^H \mathbf{a}_{m,n}}{\sigma^2}. \tag{65}$$

Since

$$\begin{aligned}\sum_{k=1}^{K-L} \mathbf{a}_{m,n}^H \mathbf{u}_k \mathbf{u}_k^H \mathbf{a}_{m,n} \mathbf{a}_{m,n} &= \mathbf{a}_{m,n}^H (\mathbf{I} - \mathbf{H}(\mathbf{H}^H\mathbf{H})^{-1}\mathbf{H}^H)\mathbf{a}_{m,n} \\ &= \mathbf{a}_{m,n}^H \mathbf{P}_{\mathbf{H}}^{\perp} \mathbf{a}_{m,n}, \end{aligned} \tag{66}$$

the above noncentrality parameter can be rewritten as $\gamma = 2|\alpha_{m,n}|^2 \sum_{k=1}^{K-L} \mathbf{a}_{m,n}^H \mathbf{P}_{\mathbf{H}}^{\perp} \mathbf{a}_{m,n}/\sigma^2$, the same as the γ of (23), which completes the proof of (32).

Similar to the H_0 case, the numerator and denominator of the GLRT test variable are correlated. In particular, since $\mathbf{u}_1 = \mathbf{q}_1$ [see (60)], we have the Gaussian variable $z_{m,n,1}$ in (63) identical to the $\zeta_{m,n,1}$ in (64), i.e., $z_{m,n,1} = \zeta_{m,n,1}$. Hence, $T_{\mathrm{GLR-Num}}$ in (31) is a part of the denominator $T_{\mathrm{GLR-Den}}$ of (30).

Finally, we provide a proof for (34). Following the calculations in (63), (64), and $z_{m,n,1} = \zeta_{m,n,1}$, we have

$$\frac{2}{\sigma^2}\left(T_{\mathrm{GLR-Den}} - T_{\mathrm{GLR-Num}}\right) = \frac{2}{\sigma^2} \sum_{m,n} \sum_{k=2}^{K-L} |\zeta_{m,n,k}|^2 \tag{67}$$

which seems to suggest that $2/\sigma^2\left(T_{\mathrm{GLR-Den}} - T_{\mathrm{GLR-Num}}\right)$ is a noncentral Chi-square variable with $2(K-L-1)MN$ degrees of freedom and noncentrality parameter $2|\alpha_{m,n}|^2 \sum_{k=2}^{K-L} \mathbf{a}_{m,n}^H \mathbf{u}_k \mathbf{u}_k^H \mathbf{a}_{m,n}/\sigma^2$. However, the noncentrality vanishes since

$$\begin{aligned}\mathbf{u}_k \perp \mathbf{u}_1 = \mathbf{b}_{m,n} &= \frac{\mathbf{P}_{\mathbf{H}}^{\perp}\mathbf{a}_{m,n}}{(\mathbf{a}_{m,n}^H\mathbf{P}_{\mathbf{H}}^{\perp}\mathbf{a}_{m,n})^{\frac{1}{2}}} \\ \Leftrightarrow 0 = \mathbf{a}_{m,n}^H \mathbf{P}_{\mathbf{H}}^{\perp} \mathbf{u}_k &= \mathbf{a}_{m,n}^H \mathbf{u}_k \end{aligned} \tag{68}$$

where the last equality is due to $\mathbf{P}_{\mathbf{H}}^{\perp}\mathbf{u}_k = \mathbf{u}_k$ (recall $\mathbf{u}_k \in \mathcal{S}_{\mathbf{H}}^{\perp}$). Hence, the difference $\frac{2}{\sigma^2}\left(T_{\mathrm{GLR-Den}} - T_{\mathrm{GLR-Num}}\right)$ reduces to a *central* chi-square variable as shown in (34). The proof for Lemma 2 is now complete.

APPENDIX IV
DISTRIBUTION RELATED TO THE GAUSSIAN

For easy references, a brief summary of the statistics related to the Gaussian distribution is provided. Similar results are discussed in [29, App. 2], which use complex distributions (e.g., complex Chi-square, complex F- and complex Beta distributions). We present the results by using the more standard real counterparts (e.g., as in Matlab).

Denote two Gaussian vectors with zero-mean and nonzero mean as $\mathbf{x} \sim \mathcal{CN}(0, \mathbf{I}_N)$ and $\tilde{\mathbf{x}} \sim \mathcal{CN}(\boldsymbol{\theta}, \mathbf{I}_N)$.

Proposition 1: The random variable $y = \|\mathbf{x}\|^2$ follows a *real* central Chi-square distribution with $2N$ degrees of freedom, i.e., $y \sim \chi^2_{2N}$.

Proposition 2: The random variable $\tilde{y} = \|\tilde{\mathbf{x}}\|^2$ follows a *real* noncentral Chi-square distribution with $2N$ degrees of freedom and noncentrality parameter $\|\boldsymbol{\theta}\|^2$, i.e., $y \sim \chi'^2_{2N}(\gamma)$, where $\gamma = \|\boldsymbol{\theta}\|^2$.

Proposition 3: The random variable $z = \frac{\chi^2_{v_1}/v_1}{\chi^2_{v_2}/v_2}$ follows a central F-distribution with parameters v_1 and v_2, where $\chi^2_{v_1}$ and $\chi^2_{v_2}$ are assumed independent with each other [28, Ch. 26]. Denote the central F-distribution as $z \sim F_{v_1,v_2}$.

Proposition 4: The random variable $\tilde{z} = \frac{\chi'^2_{v_1}(\gamma)/v_1}{\chi^2_{v_2}/v_2}$ follows a noncentral F-distribution with parameters v_1 and v_2, and noncentrality parameter γ, where $\chi'^2_{v_1}(\gamma)$ and $\chi^2_{v_2}$ are assumed independent with each other [32, pp. 135 and 415], [33, pp. 893]. Denote the noncentral F-distribution as $\tilde{z} \sim F'_{v_1,v_2}(\gamma)$.

Proposition 5: The random variable

$$\begin{aligned} t &= \frac{v_1 F_{v_1,v_2}/v_2}{1 + v_1 F_{v_1,v_2}/v_2} \\ \text{or} \quad t &= \frac{1}{1 + v_2 F_{v_2,v_1}/v_1} \\ \text{or} \quad t &= \frac{\chi^2_{v_1}/\chi^2_{v_2}}{1 + \chi^2_{v_1}/\chi^2_{v_2}} \end{aligned} \tag{69}$$

follows a central Beta distribution with parameters $v_1/2$ and $v_2/2$ [28, pp. 944-945], i.e., $t \sim \beta_{v_1/2,v_2/2}$. The PDF of the Beta distribution $\beta_{a,b}$ is

$$f(t|a,b) = \frac{1}{B(a,b)} t^{a-1}(1-t)^{b-1} \tag{70}$$

where $B(a,b)$ denotes the Beta function [28].

Proposition 6: The random variable

$$\begin{aligned} \tilde{t} &= \frac{v_1 F'_{v_1,v_2}(\gamma)/v_2}{1 + v_1 F'_{v_1,v_2}(\gamma)/v_2} \\ \text{or} \quad \tilde{t} &= \frac{1}{1 + v2/(v_1 F'_{v_1,v_2}(\gamma))} \\ \text{or} \quad \tilde{t} &= \frac{\chi'^2_{v_1}(\gamma)/\chi^2_{v_2}}{1 + \chi'^2_{v_1}(\gamma)/\chi^2_{v_2}} \end{aligned} \tag{71}$$

follows a noncentral Beta distribution with parameters $v_1/2$ and $v_2/2$ and noncentrality parameter γ [30], [31] and references therein, i.e., $\tilde{t} \sim \beta'_{v_1/2,v_2/2}(\gamma)$. The PDF of the Beta distribution $\beta'_{a,b}(\gamma)$ is

$$f(t|a,b,\gamma) = \sum_{i=0}^{\infty} P\left(i; \frac{\gamma}{2}\right) I'_t(a+i,b) \tag{72}$$

where $P(i;\gamma/2)$ is the discrete Poisson probability at i with mean $\gamma/2$, and $I'_t(a,b)$ is the derivative of the incomplete Beta function [28].

REFERENCES

[1] B. Himed, H. Bascom, J. Clancy, and M. C. Wicks, H. Fujisada, J. B. Lurie, and K. Weber, Eds., "Tomography of moving target (TMT) sensors, systems, and next-generation satellites V," in *Proc. SPIE*, 2001, vol. 4540, pp. 608–619.

[2] M. C. Wicks, B. Himed, L. J. E. Bracken, H. Bascom, and J. Clancy, "Ultra narrow band adaptive tomographic radar," in *Proc. 1st IEEE Int. Workshop Computational Adv. Multi-Sensor Adapt. Process.*, Dec. 13–15, 2005, pp. 36–39.

[3] D. W. Bliss and K. W. Forsythe, "Multiple-input multiple-output (MIMO) radar and imaging: degrees of freedom and resolution," in *Proc. 37th Asilomar Conf. Signals, Syst., Comput.*, Pacific Grove, CA, Nov. 2003, vol. 1, pp. 54–59.

[4] F. C. Robey, S. Coutts, D. Weikle, J. C. McHarg, and K. Cuomo, "MIMO radar theory and experimental results," in *Proc. 38th Asilomar Conf. Signals, Syst., Comput.*, Pacific Grove, CA, Nov. 2004, vol. 1, pp. 300–304.

[5] J. Li, P. Stoica, L. Xu, and W. Roberts, "On parameter identifiability of MIMO radar," *IEEE Signal Process. Lett.*, vol. 14, no. 12, pp. 968–971, Dec. 2007.

[6] J. Li and P. Stoica, "MIMO radar with colocated antennas," *IEEE Signal Process. Mag.*, vol. 24, no. 5, pp. 106–114, Sep. 2007.

[7] L. Xu, J. Li, and P. Stoica, "Target detection and parameter estimation for MIMO radar systems," *IEEE Trans. Aerosp. Electron. Syst.*, vol. 44, no. 3, pp. 927–939, Jul. 2008.

[8] D. R. Fuhrmann and G. S. Antonio, "Transmit beamforming for MIMO radar systems using signal cross-correlation," *IEEE Trans. Aerosp. Electron. Syst.*, vol. 44, no. 1, pp. 171–186, Jan. 2008.

[9] H. Li and B. Himed, "Transmit subaperturing for MIMO radars with co-located antennas," *IEEE J. Sel. Topics Signal Process.*, vol. 4, no. 1, pp. 55–65, Feb. 2010.

[10] E. Fishler, A. M. Haimovich, R. S. Blum, L. J. Cimini, Jr, D. Chizhik, and R. A. Valenzuela, "Spatial diversity in radars—models and detection performance," *IEEE Trans. Signal Process.*, vol. 54, no. 3, pp. 823–838, Mar. 2006.

[11] N. A. Goodman, "Optimum and decentralized detection for multistatic airborne radar," *IEEE Trans. Aerosp. Electron. Syst.*, vol. 43, no. 2, pp. 806–813, Apr. 2007.

[12] A. M. Haimovich, R. S. Blum, and L. J. Cimini, "MIMO radar with widely separated antennas," *IEEE Signal Process. Mag.*, vol. 25, no. 1, pp. 116–129, Jan. 2008.

[13] A. D. Maio and M. Lops, "Design principles of MIMO radar detectors," *IEEE Trans. Aerosp. Electron. Syst.*, vol. 43, no. 3, pp. 886–898, Jul. 2007.

[14] Q. He and R. Blum, "Cramer–Rao bound for MIMO radar target localization with phase errors," *IEEE Signal Process. Lett.*, vol. 17, no. 1, pp. 83–86, Jan. 2010.

[15] Q. He, R. Blum, H. Godrich, and A. Haimovich, "Target velocity estimation and antenna placement for MIMO radar with widely separated antennas," *IEEE J. Sel. Topics Signal Process.*, vol. 4, no. 1, pp. 79–100, Feb. 2010.

[16] H. Godrich, A. Haimovich, and R. Blum, "Target localization accuracy gain in MIMO radar-based systems," *IEEE Trans. Inf. Theory*, vol. 56, no. 6, pp. 2783–2803, Jun. 2010.

[17] C. Y. Chong, F. Pascal, J.-P. Ovarlez, and M. Lesturgie, "MIMO radar detection in non-Gaussian and heterogeneous clutter," *IEEE J. Sel. Topics Signal Process.*, vol. 4, no. 1, pp. 115–126, Feb. 2010.

[18] M. Akcakaya and A. Nehorai, "MIMO radar detection and adaptive design under a phase synchronization mismatch," *IEEE Trans. Signal Process.*, vol. 58, no. 10, pp. 4994–5005, Oct. 2010.

[19] Q. He, N. H. Lehmann, R. S. Blum, and A. M. Haimovich, "MIMO radar moving target detection in homogeneous clutter," *IEEE Trans. Aerosp. Electron. Syst.*, vol. 46, no. 3, pp. 1290–1301, Jul. 2010.

[20] J. Li and P. Stoica, *MIMO Radar Signal Processing*. Hoboken, NJ: Wiley, 2009.

[21] H. He, P. Stoica, and J. Li, "Designing unimodular sequence sets with good correlations—Including an application to MIMO radar," *IEEE Trans. Signal Process.*, vol. 57, no. 11, pp. 4391–4405, Nov. 2009.

[22] M. I. Skolnik, *Introduction to Radar Systems*, 3rd ed. New York: McGraw-Hill, 2001.

[23] N. J. Willis, *Bistatic Radar*, 2nd ed. Raleigh, NC: SciTech Publishing, 2005.

[24] J. Ward, "Space-time adaptive processing for airborne radar," Lincoln Lab., Lexington, MA, MIT Tech. Rep. 1015, 1994.
[25] L. L. Scharf and B. Friedlander, "Matched subspace detectors," *IEEE Trans. Signal Process.*, vol. 42, no. 8, pp. 2146–2157, Aug. 1994.
[26] C. D. Richmond, "Performance of the adaptive sidelobe blanker detection algorithm in homogeneous environments," *IEEE Trans. Signal Process.*, vol. 48, no. 5, pp. 1235–1247, May 2000.
[27] F. C. Robey, D. R. Fuhrmann, E. J. Kelly, and R. Nitzberg, "A CFAR adaptive matched filter detector," *IEEE Trans. Aerosp. Electron. Syst.*, vol. 28, no. 1, pp. 208–216, Jan. 1992.
[28] M. Abramowitz and I. A. Ryzhik, *Handbook of Mathematical Functions with Formulas, Graphs, and Mathematical Tables*. New York: Dover, 1972.
[29] E. J. Kelly and K. Forsythe, "Adaptive detection and parameter estimation for multidimensional signal models," Lincoln Lab., MIT, Lexington, MA, Tech. Rep. 848, 1989.
[30] H. O. Posten, "An effective algorithm for the noncentral beta distribution function," *Amer. Stat.*, vol. 47, no. 2, pp. 129–131, May 1993.
[31] R. Chattamvelli, "A note on the noncentral beta distribution function," *Amer. Stat.*, vol. 49, no. 2, pp. 231–234, May 1995.
[32] H. Scheffe, *The Analysis of Variance*, 2nd ed. New York: Wiley, 1959.
[33] A. Stuart and J. K. Ord, *Kendall's Advanced Theory of Statistics*, 6th ed. New York: Oxford Univ. Press, 1999, vol. 2A, Classical Inference and the Linear Model.

Pu Wang (M'11) received the B.Eng. and M.Eng. degrees from the University of Electronic Science and Technology of China (UESTC), Chengdu, China, in 2003 and 2006, respectively, and the Ph.D. degree from the Stevens Institute of Technology, Hoboken, NJ, in 2011, all in electrical engineering.

He was an intern at the Mitsubishi Electric Research Laboratories (MERL), Cambridge, MA, in summer 2010. Since May 2011, he has been with the Department of Electrical and Computer Engineering, Stevens Institute of Technology, Hoboken, NJ, where he is currently a Research Assistant Professor. His current research interests include statistical signal processing for multiantenna systems, nonstationary systems, wireless communications, and networks.

Dr. Wang received the Outstanding Doctoral Thesis in EE Award in 2011, the Edward Peskin Award in 2011, the Francis T. Boesch Award in 2008, and the Outstanding Research Assistant Award in 2007 from the Stevens Institute of Technology, the Excellent Master Thesis Award of Sichuan Province in 2007, and the Excellent Master Thesis Award of UESTC in 2006. He was one of the finalists in the Best Student Paper Competition at the 2011 IEEE Radar Conference.

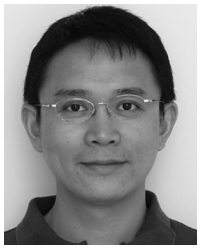

Hongbin Li (M'99–SM'08) received the B.S. and M.S. degrees from the University of Electronic Science and Technology of China, Chengdu, in 1991 and 1994, respectively, and the Ph.D. degree from the University of Florida, Gainesville, FL, in 1999, all in electrical engineering.

From July 1996 to May 1999, he was a Research Assistant in the Department of Electrical and Computer Engineering at the University of Florida. He was a Summer Visiting Faculty Member at the Air Force Research Laboratory in the summers of 2003, 2004 and 2009. Since July 1999, he has been with the Department of Electrical and Computer Engineering, Stevens Institute of Technology, Hoboken, NJ, where he is currently a Professor. His current research interests include statistical signal processing, wireless communications, and radars.

Dr. Li is a member of Tau Beta Pi and Phi Kappa Phi. He received the Harvey N. Davis Teaching Award in 2003 and the Jess H. Davis Memorial Award for excellence in research in 2001 from Stevens Institute of Technology, and the Sigma Xi Graduate Research Award from the University of Florida in 1999. He is presently a member of both the Sensor Array and Multichannel (SAM) Technical Committee and the Signal Processing Theory and Methods (SPTM) Technical Committee of the IEEE Signal Processing Society. He has served as an Associate Editor for the IEEE TRANSACTIONS ON WIRELESS COMMUNICATIONS, the IEEE SIGNAL PROCESSING LETTERS, and the IEEE TRANSACTIONS ON SIGNAL PROCESSING, and a Guest Editor for the *EURASIP Journal on Applied Signal Processing* Special Issue on Distributed Signal Processing Techniques for Wireless Sensor Networks.

Braham Himed (S'88-M'90-SM'01-F'07) received his B.S. degree in electrical engineering from Ecole Nationale Polytechnique of Algiers in 1984, and his M.S. and Ph.D. degrees both in electrical engineering, from Syracuse University, Syracuse, NY, in 1987 and 1990, respectively.

Dr. Himed is a Technical Advisor with the Air Force Research Laboratory, Sensors Directorate, RF Technology Branch, in Dayton OH, where he is involved with several aspects of airborne and spaceborne phased array radar systems. His research interests include detection, estimation, multichannel adaptive signal processing, time series analyses, array processing, space-time adaptive processing, and waveform diversity.

Dr. Himed is the recipient of the 2001 IEEE region I award for his work on bistatic radar systems, algorithm development, and phenomenology. Dr. Himed is a fellow of the IEEE and a member of the AES Radar Systems Panel.